Transition from continental break-up to punctiform seafloor spreading: How fast, symmetric and magmatic

Giacomo Corti,[1,2] Jolante Van Wijk,[3,4] Marco Bonini,[5] Dimitrios Sokoutis,[3] Sierd Cloetingh,[3] Fabrizio Innocenti,[1] and Piero Manetti[6]

[1] We present a comparison between numerical and analogue models focusing on the role of inherited lithospheric structures in influencing the process of continental break-up. Our results highlight that the presence of pre-existing anisotropies localizes strain and favors continental break-up and formation of a new ocean. For a fixed strain rate, the pre-rift lithosphere configuration influences rift duration, melt production and width and symmetry of the continental margin pair. Model results show a mainly two-phase tectonic history from continental extension to oceanization. In the first phase extension affects contemporaneously the whole rift structure, while in the second phase asthenosphere upwelling occurs into punctiform regularly-spaced spots sequentially propagating in an extension-orthogonal direction. *INDEX TERMS:* 8109 Tectonophysics: Continental tectonics—extensional (0905); 8120 Tectonophysics: Dynamics of lithosphere and mantle—general; 8150 Tectonophysics: Plate boundary—general (3040). **Citation:** Corti, G., J. Van Wijk, M. Bonini, D. Sokoutis, S. Cloetingh, F. Innocenti, and P. Manetti, Transition from continental break-up to punctiform seafloor spreading: How fast, symmetric and magmatic, *Geophys. Res. Lett.*, *30*(12), 1604, doi:10.1029/2003GL017374, 2003.

1. Introduction

[2] Continental rifting represents the thermo-mechanical process by which continents break. If successful, this process ends with the formation of a new ocean bordered by a pair of passive margins. Duration of rifting as well as the characteristics of the resulting margins (volcanicity, width and symmetry) are highly variable. Rift duration prior to break-up and crustal separation is suggested to vary between 9 and 280 My, although not all the rifts are successful and some of them are aborted [*Ziegler and Cloetingh*, 2003]. About 90% of the passive margins are volcanic whereas the remaining 10% are non-volcanic with only limited amounts of volcanic rocks [*Menzies et al.*, 2002]. Some margins are wide while others are narrow [*Davison*, 1997]; pairs of passive margins may be symmetric (narrow-narrow or wide-wide) or asymmetric (narrow-wide). Observations of margin volcanicity and margin geometry (width and symmetry) show that a systematic relation does not exist. Models formulated to explain such a structural variability consider differences in [e.g., *Davison*, 1997]: 1) initial rheological or thermal structure of the lithosphere, 2) rift kinematics, 3) strain rate, 4) melt volumes at a margin, 5) presence of pre-existing weakness zones and 6) development of large detachment faults. Processes controlling volcanicity at passive margins include the interaction of mantle plumes with the lithosphere [*White*, 1992], small thermal anomalies in the mantle with no mantle plumes [*Anderson*, 2000] and convective upwelling of mantle material into the melting zone during rifting (small-scale convection models) [e.g., *Boutilier and Keen*, 1999]. *Van Wijk et al.* [2001] suggested that volcanic margins may result from high extension velocities, whereas *Dunbar and Sawyer* [1989] and *Harry and Bowling* [1999] suggested that the pre-existing lithosphere structure may be a controlling factor on volcanicity of passive margins. Indeed, the geological record suggests that rifting processes often localize along ancient orogenic belts and suture zones [*Dunbar and Sawyer*, 1989]: By weakening the crust, these pre-existing crustal discontinuities play a major role in the localization and distribution of crustal strain.

[3] In this study we analyze the role of inherited lithospheric weakness zones in influencing the continental break-up process, in terms of 1) rift duration, 2) melt production, 3) geometry of the resulting margins and 4) the 3D evolution of the oceanization process. We approach the problem through comparison of numerical models and analogue experiments. In order to compare the results, both analogue and numerical models simulated a similar lithospheric rheology and the same extension rate of ∼30 mm/yr, which falls within the range of present day plate velocities [*Argus and Heflin*, 1995].

2. Numerical Modeling

[4] Lithosphere extension in relation to the inherited Moho topography was investigated in numerical models using a two-dimensional finite element model [*Van Wijk et al.*, 2001]. The Lagrangian formulation was used and the finite element grid was periodically remeshed. Visco-elastic behavior of the lithosphere was described by a Maxwell body [*Turcotte and Schubert*, 1982]:

$$\dot{\varepsilon} = \frac{1}{2\mu}\sigma + \frac{1}{E}\frac{d\sigma}{dt} \qquad (1)$$

---

[1]Dipartimento di Scienze della Terra, Univ. di Pisa, Italy.

[2]Now at Dipartimento di Scienze della Terra, Univ. di Firenze, Italy.

[3]Netherlands Center for Integrated Solid Earth Science, Vrije Univ. Amsterdam, The Netherlands.

[4]Now at IGPP Scripps Institution of Oceanography, Univ. of California, San Diego.

[5]C. N. R., Istituto di Geoscienze e Georisorse, Sezione di Firenze, Italy.

[6]C. N. R., Istituto di Geoscienze e Georisorse, Pisa, Italy.

where $\dot{\varepsilon}$ is strain rate, μ is dynamic viscosity, σ is stress and E is Young's modulus. The non-linear relation between stress and strain rate was described by:

$$\dot{\varepsilon} = A\sigma^n \exp\frac{-Q}{RT} \qquad (2)$$

where A, n (power law exponent) and Q (activation energy) are experimentally derived material constants [*Carter and Tsenn*, 1987; *Ranalli*, 1995], R is the gas constant and T is temperature. The state of stress is constrained by the force balance:

$$\nabla\sigma + \rho g = 0 \qquad (3)$$

where g is gravity and ρ is density. In the model, the density is dependent on the temperature following a linear equation of state: $\rho = \rho_0(1 - \alpha T)$, where ρ_0 is the density at the surface, α is the thermal expansion coefficient and T is temperature. Yield conditions were described by the Mohr-Coulomb criterion. The empirically derived equations for dry mantle peridotite of *McKenzie and Bickle* [1988] were used to calculate melt generation due to decompressional partial melting during extension of the lithosphere, whereby migration of melt was not implemented. Neither the influence of melt on the density nor on the viscosity are included in the model, which means that only first-order melt volumes are predicted. We did not incorporate sedimentation and erosion in the model.

[5] The influences of the initial Moho topography on the rifting process, was studied by testing several different pre-rift Moho configurations in the models (see Figure 1a). The differences between the Moho configurations were not very large; such small variations are very likely to exist almost everywhere. Both symmetric and asymmetric initial Moho geometries were considered. Other initial boundary conditions, as well as the rheology were the same for the tests performed, so differences in the rift evolution were expected to be caused by the prescribed Moho configuration. The lithosphere was stretched until a maximum crustal thinning factor of 20 was reached.

[6] Numerical modeling results suggest that, for the given initial boundary conditions, the duration of break-up as well as the width of the margin pair are influenced by the width of the initial perturbations in lithospheric strength, with narrow Moho anomalies (e.g., models MT A and MT F; Figure 1b, Table 1) triggering a rapid continental break-up, with resulting narrow margins. An increase in the width of the Moho anomaly results in a larger rift duration and larger melt production, due to a wider mantle upwelling area (Table 1). However, models show that there is an upper limit in pre-rift Moho anomaly above which melt production does not occur (MT C; Figure 1b, Table 1). Thus, Moho topography influences the thermal structure during and after rifting, the amount of decompressional partial melting and hence the volcanicity or non-volcanicity of passive margins. The influence of the pre-rift lithospheric structure may also influence the along-axis variations in melt production documented in many margins, a feature that is more difficult to explain with models invoking variations in the extension velocity or warm mantle plumes near the rift structure. Symmetry/asymmetry of the margin pairs is also largely influenced by the pre-rift lithosphere configuration: An
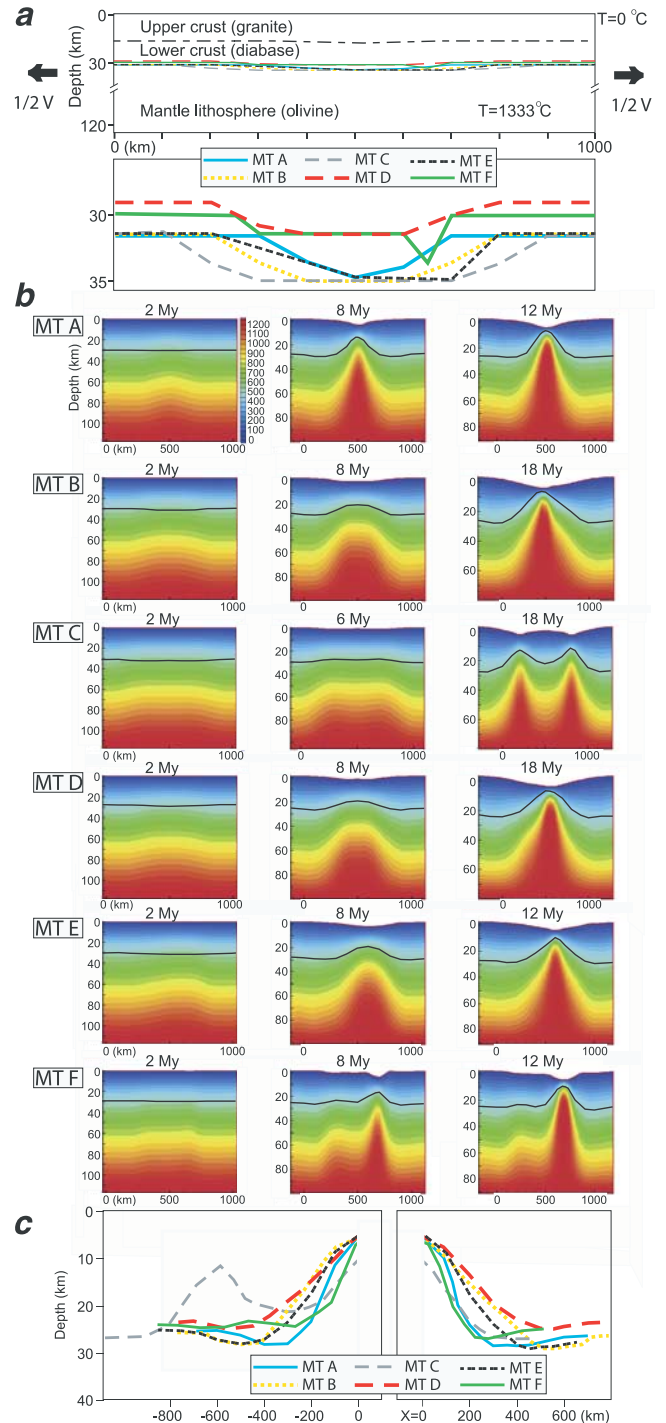

Figure 1. (a) Pre-rift lithosphere configuration used for the numerical modeling (upper panel), vertical scale exaggerated (lower panel). V is total extension velocity. (b) Thermal evolution for the different models MT A-F. Time in My after stretching of the lithosphere began. Temperature (°C) scale is the same for all panels. The black line in each panel shows the Moho. (c) Model predicted Moho depths of two conjugate margins for tests A-F at the time when a crustal thinning factor of 20 was reached (see Table 1). X = 0 is the location where a crustal thinning factor of 20 was reached first.

Table 1. Numerical Modeling Results for Models MT A to F[a]

Model	Rift duration (My)	Melt volume (km3)	Margin width (km)	Symmetry
MT A	12	975	~300	Symmetric
MT B	18	1275	~500	Symmetric
MT C	25	70(left) and 135(right)	~400 and ~900	Asymmetric
MT D	18	700	~50	Symmetric
MT E	16	700	~400 and 500	Asymmetric
MT F	12	650	~200 and 600	Asymmetric

[a]Rift duration is the time until crustal thinning factor of 20 is reached. Melt volume is volume per km along strike of the margin. Width is width of margin to the largest Moho depth (Figure 1). Symmetry relates to predicted Moho configuration as well as to thermal structure.

asymmetric pre-rift Moho profile results in an asymmetric margin pairs; for symmetric pre-existing Moho, symmetric margins are expected, although very wide initial Moho perturbations may result in an a wide/narrow (asymmetric) final configuration of the resulting margins (MT C; Figure 1c; Table 1).

3. Analogue Modeling

[7] Experimental models were deformed in an artificial gravity field of 200g at the HRTL of Uppsala Univ. to simulate extension of a three-layer system (the continental lithosphere) floating above a low-viscosity fluid (representing the asthenosphere; Figure 2a). The models simulated a pre-existing low-strength region in the lower crust (weak lower crust, WLC; Figure 2a), and were built considering the scaling ratios of length ($l^* \approx 1.5 \times 10^{-7}$; where the asterisk is the ratio between model, l_m, and nature, l_n) and gravitational stresses ($\sigma^* = \rho^* g^* l^*$, where ρ and g are density and gravity). Dynamic similarity has been achieved through dimensionless ratios of forces [*Ramberg*, 1981], and tested by scaling to nature the resistance of the lithosphere and the forces driving extension. The resistance of the brittle/ductile model multilayer has been calculated by integrating the differential stresses with depth:

$$R_L = \int_0^H (\sigma_1 - \sigma_3)(z) dz \qquad (4)$$

where R_L represents a force per unit width. The model-to-nature ratio of the resistance can be obtained by assuming that $R_L^* = \sigma^* l^*$, yielding a total resistance of the natural lithosphere R_L of $1.9-2.2 \times 10^{12}$ Pa m. With a similar scaling ratio ($\sigma^* l^*$) we have estimated the forces driving extension, which are calculated as the integrated lateral pressure variation at the free model boundaries:

$$F_d = \int_0^H \Delta P(z) dz. \qquad (5)$$

[8] Scaling to nature allows to estimate F_d values of $3-7 \times 10^{13}$ Pa m. Both R_L and F_d are in the same order of magnitude of lithospheric resistance and driving forces reported for nature, respectively [e.g., *Ranalli*, 1995], thus supporting the dynamic-cinematic similarity of the experimental approach.
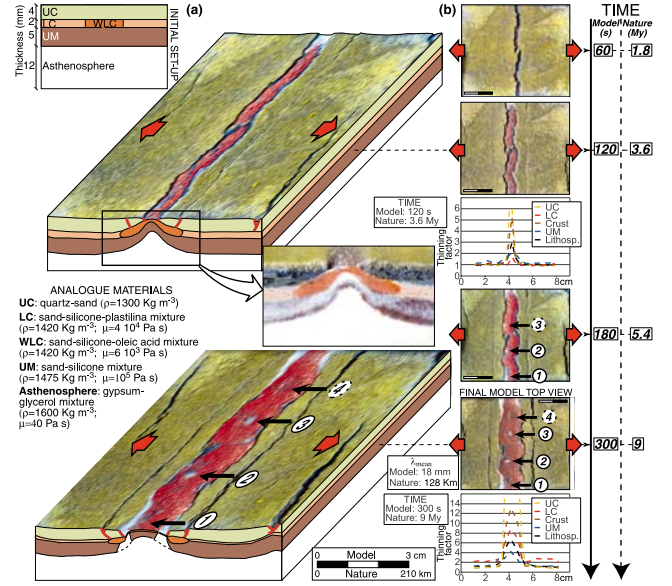

Figure 2. Analysis of deformation of analogue model CBr01. (a) Initial rheological stratification. (b) Top view photos of the model during successive deformation stages with the graphs of the thinning factors for the different layers plotted against the distance across the model. Black arrows and numbers indicate the sequential emplacement of the asthenospheric spots at surface. Orange arrows indicate the direction of extension. LC: Lower crust; UC: Upper crust; UM: Upper lithospheric mantle; WLC: Weak lower crust.

[9] Analysis of model results shows that the WLC strongly localized deformation and favored major asthenospheric upwelling below the main deformed zone, characterized by relevant lithospheric thinning (Figure 2b). For increasing extension, the asthenosphere reached the surface in regularly-spaced spots propagating from one side of the model to the other, in an extension-orthogonal direction (Figure 2b). Plot of deformation zone width versus time highlights that the presence of the WLC (model CBr01) favors a linear increase in the deformed zone width (Figure 3). Thus, extension is progressively accommodated by widening of the initial deformed zone, without lateral migration of
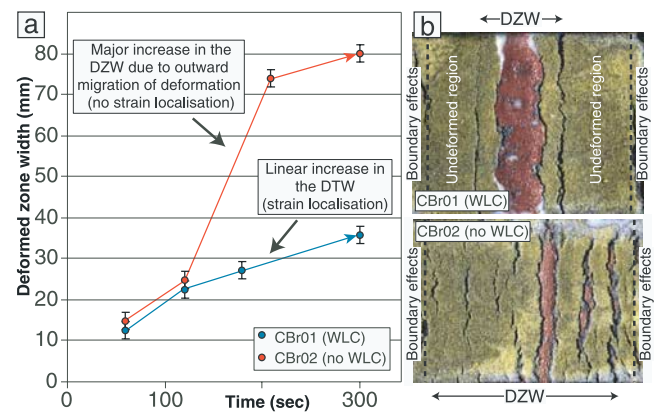

Figure 3. (a) Diagram plotting the deformed zone width versus time for models CBr01 and CBr02. (b) Final top-view photo of the models. DZW: Deformed zone width.

deformation. This feature configures a lithospheric-scale strain localization and a stable deformation process resulting in narrow rifting [*Benes and Davy*, 1996]. Conversely, the absence of WLC (model CBr02) leads to a step-like increase in the deformed zone width in time, as a result of outward jumping of deformation front into undeformed regions during progressive extension. This indicates that, for the assumed boundary conditions, a homogeneous lower crust inhibits strain localization but promotes an unstable extension process resulting in a distributed deformation zone and wide rifting. In this case, the process of continental extension does not give rise to significant thinning of the lithosphere, thus preventing the upraising of the asthenosphere.

4. Discussions and Conclusions

[10] In study we have used numerical and analogue models to investigate the process continental break-up and the characteristics of the resulting passive margin pair. Numerical models allow to model thermal variations and related melt production during rifting and to investigate the effect of even small-variations in the geometry of the inherited crustal structure on the break-up process. On the other side, analogue modeling provides a 3D picture of the evolution of the asthenosphere-lithosphere system during the break-up but simplified the thermo-mechanical process of continental extension to an isothermal (purely mechanical) process. Both analogue and numerical modelling suggest that the pre-rift lithosphere configuration is able to control the continental rifting to a large extent. Particularly, inherited weakness zones initiate strain localization that, coupled to a favorable plate kinematics, leads to a successful continental break-up. 2D numerical models highlight that, for a fixed extension rate, the duration of the break-up process, the amount of melt generated and the structure (width and symmetry) of the resulting passive margin pairs are largely controlled by even small variations in the initial Moho topography. The 3D picture of the break-up process provided by the analogue model outlines a two-phase tectonic history. In the first phase extension takes place contemporaneously along the whole rift structure, while the progressive propagation of periodic asthenospheric instabilities in an extension-orthogonal (along-strike) direction characterizes the second phase. In this case, extension of the model lithosphere triggers the development of a sinusoidal instability determining regularly-spaced injections of a lower viscosity fluid (asthenosphere) into an overlying more viscous layer (lower crust + lithospheric mantle). Scaling to nature of the instabilities wavelength in the model, yields a value of $\lambda \approx 130$ Km, which well correlates with values observed in some oceanic ridges [*Bonatti*, 1985]. This process is substantially analogous to the punctiform seafloor spreading proposed by *Bonatti* [1985] for the Red Sea. Thus, the current modeling supports that seafloor spreading in the Red Sea resulted from a two-phase evolution, in which (1) the Miocene continental extension affecting simultaneously the entire rift length was followed by (2) the Pliocene northward (i. e., extension-orthogonal) activation of the hot points leading to oceanization [*Bonatti*, 1985; *Omar and Steckler*, 1995].

References

Anderson, D. L., The thermal state of the upper mantle: No role for mantle plumes, *Geophys. Res. Lett.*, *27*, 3623–3626, 2000.

Argus, D. F., and M. B. Heflin, Plate motion and crustal deformation estimated with geodetic data from the Global Positioning System, *Geophys. Res. Lett.*, *22*, 1973–1976, 1995.

Benes, V., and P. Davy, Modes of continental lithospheric extension: Experimental verification of strain localization processes, *Tectonophysics*, *254*, 69–87, 1996.

Bonatti, E., Punctiform initiation of seafloor spreading in the Red Sea during transition from a continental to an oceanic rift, *Nature*, *316*, 33–37, 1985.

Boutilier, R. R., and C. E. Keen, Small-scale convection and divergent plate boundaries, *J. Geophys. Res.*, *104*, 7389–7403, 1999.

Carter, N. L., and M. C. Tsenn, Flow properties of continental lithosphere, *Tectonophysics*, *136*, 27–63, 1987.

Davison, I., Wide and narrow margins of the Brazilian South Atlantic, *J. Geol. Soc. London*, *154*, 471–476, 1997.

Dunbar, J. A., and D. S. Sawyer, Continental rifting at pre-existing lithospheric weaknesses, *Nature*, *242*, 565–571, 1989.

Harry, D. L., and J. C. Bowling, Inhibiting magmatism on nonvolcanic rifted margins, *Geology*, *27*, 895–898, 1999.

McKenzie, D. P., and M. J. Bickle, The volume and composition of melt generated by extension of the lithosphere, *J. Petrol.*, *29*, 625–679, 1988.

Menzies, M. A., S. L. Klemperer, C. J. Ebinger, and J. Baker, Characteristics of volcanic rifted margins, in *Volcanic rift margins*, edited by M. A. Menzies, S. L. Klemperer, C. J. Ebinger, and J. Baker, *Spec. Pap. Geol. Soc. Am.*, *362*, 1–14, 2002.

Omar, G. I., and M. S. Steckler, Fission track evidence on the initial rifting of the Red Sea; two pulses, no propagation, *Science*, *270*, 1341–1344, 1995.

Ramberg, H., Gravity, Deformation and the Earth's Crust, 452 pp., Academic, San Diego, California, 1981.

Ranalli, G., Rheology of the Earth, 413 pp., Chapman and Hall, New York, 1995.

Turcotte, D. L., and G. Schubert, *Geodynamics: Applications of continuum physics to geological problems*, 450 pp., Wiley, New York, 1982.

Van Wijk, J. W., R. S. Huismans, M. ter Voorde, and S. Cloetingh, Melt generation at passive continental margins: No need for a mantle plume?, *Geophys. Res. Lett.*, *28*, 3995–3998, 2001.

White, R. S., Magmatism during and after continental break-up, in *Magmatism and the Causes of Continental Break-up*, edited by B. C. Storey, T. Alabaster, and R. J. Pankhurst, *Geol. Soc. Spec. Publ.*, *68*, 1–16, 1992.

Ziegler, P., and S. Cloetingh, Dynamic processes controlling evolution of rifted basins, *Earth Sci. Rev.*, in press, 2003.

————————————

M. Bonini, C. N. R., Istituto di Geoscienze e Georisorse, Sezione di Firenze, via La Pira, 4, 50121 Firenze, Italy.

S. Cloetingh and D. Sokoutis, Netherlands Center for Integrated Solid Earth Sciences, Faculty of Earth and Life Science, Vrije Univ. Amsterdam, De Boelelaan 1085, 1081 HV, Amsterdam, The Netherlands.

G. Corti, Dipartimento di Scienze della Terra, Univ. di Firenze, via La Pira, 4, 50121, Firenze, Italy. (cortigi@geo.unifi.it)

F. Innocenti, Dipartimento di Scienze della Terra, Univ. di Pisa, via S. Maria, 53, 56126 Pisa, Italy.

P. Manetti, C. N. R., Istituto di Geoscienze e Georisorse, via G. Moruzzi, 1, 56124 Pisa, Italy.

J. Van Wijk, IGPP Scripps Institution of Oceanography, Univ. of California, San Diego, La Jolla, CA 92093-0225, USA.